Design and Fabrication of a Prototype Scintillating Fiber Tagger Microscope for the GlueX Experiment

I. Senderovich, C.R. Nettleton, M. Underwood and R.T. Jones

September 15, 2008

Abstract

The University of Connecticut nuclear physics group has made significant progress in finalizing the design of the scintillating fiber tagging counters for the Hall D 12 GeV photon tagger at Jefferson Lab. A SiPM photo-detector for the fiber readout meeting all of the tagged beam specifications has been identified and tested in detail in terms of its detection efficiency, gain, thermal noise, as well as sensitivity to temperature and variation in bias voltage. Base electronics for bias of these devices and amplification of their signals have been designed and laid out. Likewise, electronics for monitoring and individual SiPM bias control have been designed, laid out and submitted for fabrication. The communication protocol with these boards has been defined and programmed in the form of a FPGA core. Procedures for the cutting, polishing and gluing of fibers for optimal scintillation light capture and minimal optical cross-talk have been refined to enable the fabrication of a prototype detector subtending 5% of the full microscope. The group has designed the necessary mechanical features for a light-sealed detector enclosure, motorized fiber array alignment control and mounting of SiPM amplifier boards as well as their coupling to optical corresponding fiber bundles. Work on machining the parts for the prototype is underway.

1 Overview

A polarized photon beam with energies up to 12 GeV will be produced in the future Hall D at Jefferson Lab using coherent bremsstrahlung (CB) of electrons in a diamond crystal. Coherent scattering from planes in the diamond crystal structure produces enhancements in the radiation spectrum in the form of distinct peaks on top of the incoherent background. The peak of greatest interest to the GlueX experiment is the one associated with the (2,2,0) planes of the diamond crystal. When the crystal is suitably oriented in the 12 GeV electron beam, this peak appears as an enhancement in the beam intensity spectrum in the energy region 8.4 - 9.0 GeV. This peak is further enhanced by the use of collimation to a factor 7 in intensity above the incoherent background, as shown in Fig. 1, with 40% linear polarization in the region of the peak.

The energy of the photon is tagged by measuring the energy of the electron after radiation. A magnetic spectrometer is placed downstream of the diamond radiator. The electron focal plane generated by the magnet is instrumented with two focal plane arrays: the broad-band hodoscope and a narrow-band microscope. The corresponding spectral bands are shown in Fig. 1. The microscope was conceived as a device capable of higher tagging rates, higher energy resolution and vertical focal plane position segmentation to discriminate against out-of-plane photons that fall outside the collimator acceptance.

Rate considerations require focal plane segmentation into bins of 8 MeV, which translates into counter widths of 2 mm at the tagger focal plane between 8 and 9 GeV. The kinematic projection of the photon collimator onto the electron impact positions at the focal plane produces a stripe about 2 mm high. Thus, segmentation of the tagger microscope into cells of dimension 2×2 mm^2 satisfies the dual requirements of adequate energy segmentation and vertical position resolution. This geometry is achieved by stacking square scintillating fibers of transverse size 2×2 mm^2 in a close-packed array 5 high and 100 wide. Scintillating fibers for 2 cm-long segments aligned with electron trajectories, so that tagging electrons pass axially down the fiber where they deposit an average of 4 MeV. The length of 2 cm has been chosen to achieve good timing resolution in these counters, while minimizing the sharing of energy between adjacent channels which results from multiple scattering in the scintillator. A clear fiber waveguide of matching cross-section is coupled to the each scintillator and connected to a photo-sensor located out of the plane of the electrons. Instead of the conventional choice of photomultiplier tubes (PMTs), Silicon Photomultipliers (SiPMs) have been selected for this role due to their matching active area to the fiber cross-section, fast response, orders of magnitude smaller bias and insensitivity to magnetic fields. A more detailed discussion of the design choices summarized above can be found in an earlier report. [1]

2 Requirements

Table 1 summarizes the tagged photon beam requirements for Hall D which have a direct impact on the design of the tagging microscope. Meeting these specifications is essential for the physics goals set forth by the GlueX experiment.

3 Design and Prototyping of SiPM Base Electronics

3.1 SiPM Characterization

Research into the suitability of the SiPM for tagger use and identification of Photonique's SSPM-0606BG4-PCB as the best candidate currently available on the market has been documented in previous reports from this group. [1] The development and testing of the requisite bench-top equipment for the purposes of SiPM characterization, light source characterization techniques and signal normalization has also been discussed in detail. Additional new results concerning the test stand stability have been attached as an appendix to this document. (App. A)

Further measurements were made to determine the sensitivity of SSPM-0606BG4-PCB (shown in Fig. 2) to ambient temperature and bias voltage. The test stand was used to measure the SiPM

Table 1: Requirements for the performance of the tagger microscope derived from the physics goals of the GlueX experiment, matched up with the corresponding design specification for the tagger microscope.

requirement	design specification
coverage within coherent peak 8.4-9.0 GeV	cover the region in electron energy 2.90-3.70 GeV to bracket the coherent peak at 12 GeV electron beam energy
tagging time resolution better than 200 ps r.m.s.	minimum 200 photoelectrons per pulse, where n-photon group arrival time spread goes as $\tau/\sqrt{n}$, with single photon arrival time uncertainty τ set principally by scintillator decay time, τ =2.7 ns for BCF-20 [a]
average tagging efficiency as high as possible, at least 30%	tagging efficiency 70% averaged within the coherent peak [b]
tagging at rates up to 10^8 tags/s in coherent peak	less than 5% detector and readout occupancy at 10^8 tags/s [c]
tagger energy resolution better than 0.5% of 9 GeV	superseded by the per-channel rate limitation, resulting in an average channel width of 8 MeV
capable of operation at 10^{-3} nominal intensity for absolute normalization measurements	net dark rate over threshold for all channels less than 1 Hz [d]

[a] Optimization of detected light is discussed in terms of optics in Sec. 4, and photo-detector efficiency in Sec. 3.1.
[b] Achieved using vertical segmentation of the focal plane counters.
[c] Achieved by minimizing photo-detector dead time. SiPMs now offer just 15 ns recovery time. Signal stretching due to amplifier RC time is being reduced (Sec. 3.3).
[d] This is a constraint on the rate of spurious SiPM pulses which result from transients, cosmic ray background and device-specific "dark pulses" due to thermal electronic noise (Sec. 3.1).

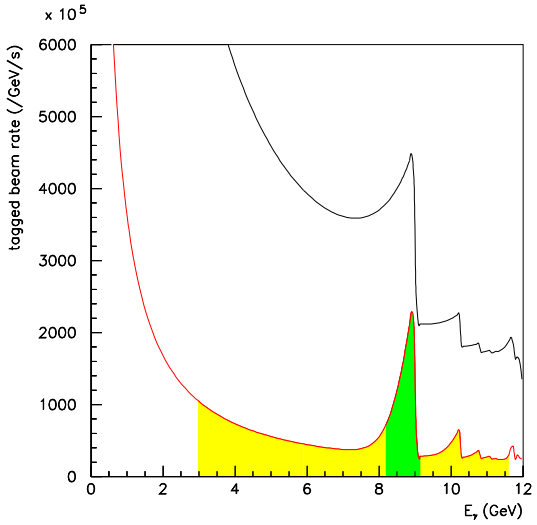

Figure 1: Coherent bremsstrahlung beam spectrum from 12 GeV electrons at the current foreseen for full-intensity running with the Hall D tagged beam. The upper curve represents the rates seen in the tagging counters, while the lower curve is the spectrum of the photons passing through the collimator. The broad shaded region shows the range tagged by the broad-band hodoscope. The narrow shaded region represents the energies tagged by the microscope.

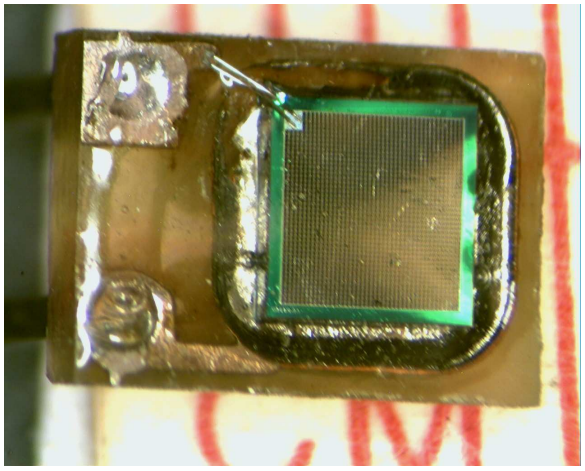

Figure 2: Photonique SSPM-0606BG4-PCB (4.4 mm^2 - 1700 pixels)

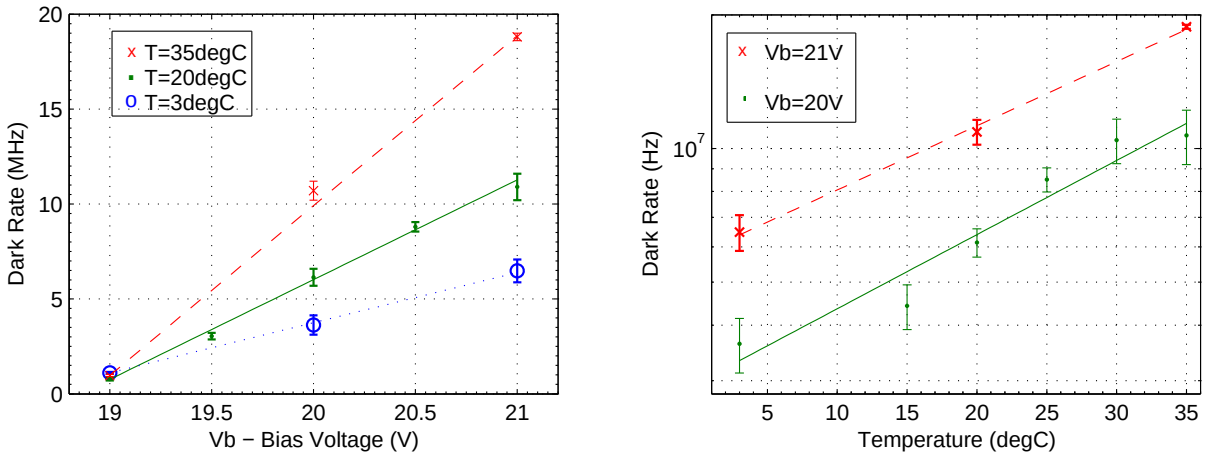

Figure 3: Dark rate plotted as a function of bias voltage at extreme and room temperatures (first panel), and as a function of temperature at different bias voltages (second panel).

efficiency, gain, and dark rate as a function of temperature (T) and bias voltage (V_b). Several points in the T, V_b parameter space were sampled. Bias voltages of 19 V, 20 V and 21 V were tested, covering values in the neighborhood of the nominal operating range of 19.5 V - 20.5 V. In the degree of freedom of temperature, samples were taken at 3°C, 20°C and 35°C. A more detailed scan in temperature was performed at V_b =20 V, and a more detailed scan in bias voltage was carried out at 20°C. Figs. 3-5 show the results of these scans.

The data shows that both gain and detection efficiency improve with higher bias voltage and lower temperature. As expected, the dark rate increases with temperature and bias voltage. The tests confirm that at the recommended bias voltage (at or below 20.5 V) and at room temperature these devices satisfy the performance requirements for the tagger microscope. Their PDE, gain, and dark rate are all regular and smooth functions of temperature within 15°C of room temperature and of bias voltage within ±1 V of the recommended V_b. Tuneability of V_b within ±0.1 V is desirable in order to match the operating characteristics between different channels and maintain a good degree of uniformity in the response across the microscope.

The dark rates advertised by the manufacturer and confirmed in these measurements should pose no problem for the tagger system. Even at a dark rate of 20 MHz, barely attainable at highest bias voltages in range with ambient temperature of 35°C, and considering a pessimistic 50% crosstalk rate characteristic of a defective device yields a false rate above 50 pixel threshold of only about 8×10^{-7} Hz. Our test setup with the SiPM set at the highest bias voltage was set to trigger on events about 35-50 pixels and above. No such events were detected in a 24 hour run. This is equivalent to a rate of 2.7×10^{-5} Hz at a confidence level of 90%. Such rates will be insignificant compared to that due to cosmic ray background and electronic noise in the form of transients.

The last SiPM studied was the Hamamatsu MPPC S10362-11-050C. Despite a 1 mm^2 active

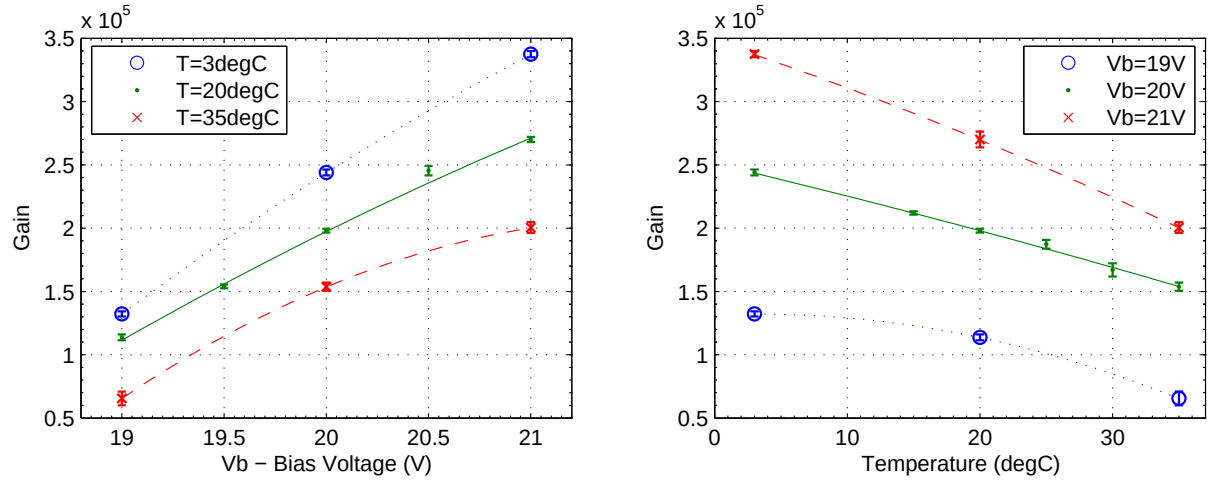

Figure 4: SiPM gain plotted as a function of bias voltage at extreme and room temperatures (first panel) and as a function of temperature at different bias voltages (second panel).

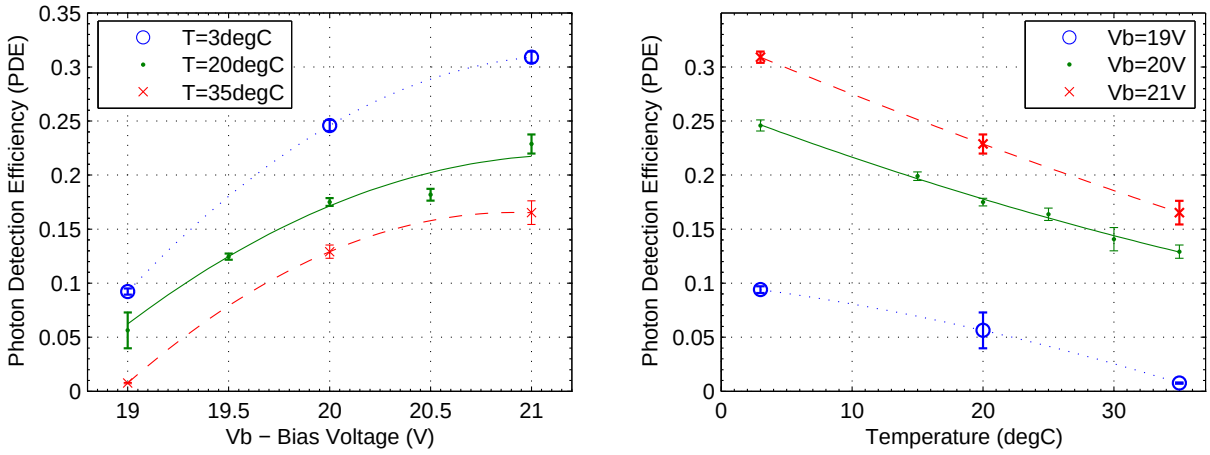

Figure 5: Photon detection efficiency as a function of bias voltage at extreme and room temperatures (first panel) and as a function of temperature at different bias voltages (second panel).

area, the device seemed promising due to its high quoted figures for gain and detection efficiency compared to the Photonique devices. The device has an especially high efficiency in the emission range of the fast blue BCF-10 scintillating fiber It was thought that the higher efficiency from this scintillator-detector pair might make up for incomplete coverage of the fiber waveguide cross-sectional area.

A statistical analysis was performed on the data from the MPPC test. It was immediately evident that the multi-Poisson model that was used to fit the Photonique SiPM's in the earlier studies referenced above could not produce satisfactory fits for this device. Individual peaks in the charge spectrum did not appear to be symmetric: they possessed a significantly longer left-hand tail. A new model was devised for the spectra from this device that produced satisfactory fits on the lower end of the spectrum. It was clear, however, that the multi-Poisson model could not describe the higher end of the spectrum. Essentially, the distribution did not fall off quickly enough in the limit of higher pixel count. Most pronounced at higher bias voltages, but present even down to threshold, this high-end tail seemed to arise from effects unrelated to primary count or cross-talk statistics. A visual examination of the wave-forms from the MPPC showed a significant number of saturated pulses coming from the simultaneous firing of all (or most) of the pixels in the device, and also significant after-pulsing. The latter is of particular concern in a tagging counter since they contribute directly to the tagging inefficiency. From these tests, it appears likely that these cross-talk effects are artificially inflating the published PDE value that is quoted by the manufacturer. In summary, it does not appear that these Hamamatsu MPPC devices are suitable for use in the tagger microscope.

3.2 Control Electronics

To satisfy the requirement of individual SiPM bias voltage control and monitoring of on-board voltages and temperature, the following scheme was devised. The SiPMs will be mounted in sets of 25 on circuit boards, which also house the analog amplifier and sum circuitry for each tagger channel. A separate circuit board containing the associated digital control electronics will be paired with each analog amplifier board, connected through the main bus-board. A diagram of the control and readout scheme is shown in Fig. 6.

The control boards will be equipped with a 32-channel DAC with an output voltage range up to 150 V, which more than covers the range in breakdown voltage foreseeable for a SiPM device. Each DAC channel is individually programmable with 14 bits of precision, which gives better than the required ± 0.1 V control over V_b on each individual SiPM. The board will also be instrumented with a temperature sensor and an 8-channel 12-bit ADC to monitor all the critical reference voltages on the board, as well as one channel of the DAC. Connection between the control boards and the outside world is over standard 10-baseT Ethernet. Ethernet was chosen for the following reasons:

1. ubiquity - Ethernet components are readily available on the consumer market.

2. high-level interface - Controllers are readily available that implement the low-level signaling and address filtering, presenting an asynchronous packet-level interface to the user's i/o controller.

3. robustness - The controller automatically negotiates the link parameters and detects errors, resending packets when necessary and performing integrity checks.

4. flexible addressing - It supports both one-to-one and one-to-many communication that is convenient for device initialization.

5. flexible interconnects - Ethernet cabling and switching provides an abundance of options for interconnects and no distance limits.

An Ethernet Controller chip (EC) will be placed on each control board. The core of the digital board design board will be an FPGA (Field Programmable Gate Array), a convenient and reliable choice for a micro-controller that will interface with all of the above components.

Issues of mapping a MAC address to the corresponding control board (representing some known SiPM channel group) have been carefully considered. The current scheme mandates that each control board connection slot be hard-wired with an 8-bit location address, with which all communication packets must be stamped. Upon initialization or in response to a special "census" broadcast, each control board sends a standard identification packet to the controlling PC, thereby announcing its presence and associating its hardware slot number to its unique MAC address. The map from SiPM position on a given readout board to the (x, y) index of the associated fiber must be recorded manually during detector assembly, and looked up in a table.

The above scheme requires an on-board EEPROM chip to provide non-volatile storage for the FPGA core. The EEPROM, in turn, is programmed via an on-board JTAG interface.

All of the chips needed for the above-described functional design have been selected. The core firmware for the FPGA has been written and "fitted" within the resources of the selected Xilinx chip. The design exhausts neither its "slices" nor its input-output blocks (IOBs). Significant numbers of both resources remain, so that future improvements to the functionality of the board should be possible in the form of firmware upgrades.

A mechanical design that allows easy replacement of failed electronics boards has been developed in which the control and amplifier boards are connected across an interconnect "backplane" board, which serves as a light-sealing panel on the top of the microscope enclosure. The chassis contains 20 such hatches to be sealed by these backplanes. The alignment of the ends of the clear fibers to the active area of the SiPM's is accomplished by a mechanical structure called the "chimney", illustrated in Fig. 14. Precise position of the chimney with respect to the hatch allows for exact alignment of the amplifier board relative to the fibers, once the backplane board is inserted and tightened against the microscope housing. The chimney structure provides a card guide for the insertion of the preamplifier in order to guarantee this alignment. This scheme allows maintenance to be performed on the electronics without disturbing the optics and is conveniently modular. Significant cost savings are foreseen in manufacturing 20 small, simple, generic backplanes instead of a single large backplane with 20 interconnects and long bussed power lines. Care will have to be taken in light-sealing the surface of the backplane PCB's to be sure that ambient light does not leak into the dark box and increase the dark rate of the SiPM's.

The group has obtained access to the requisite licenses for the Altium Designer, a CAD software suite used for circuit board layout and has carried on extensive work in layout and optimization of

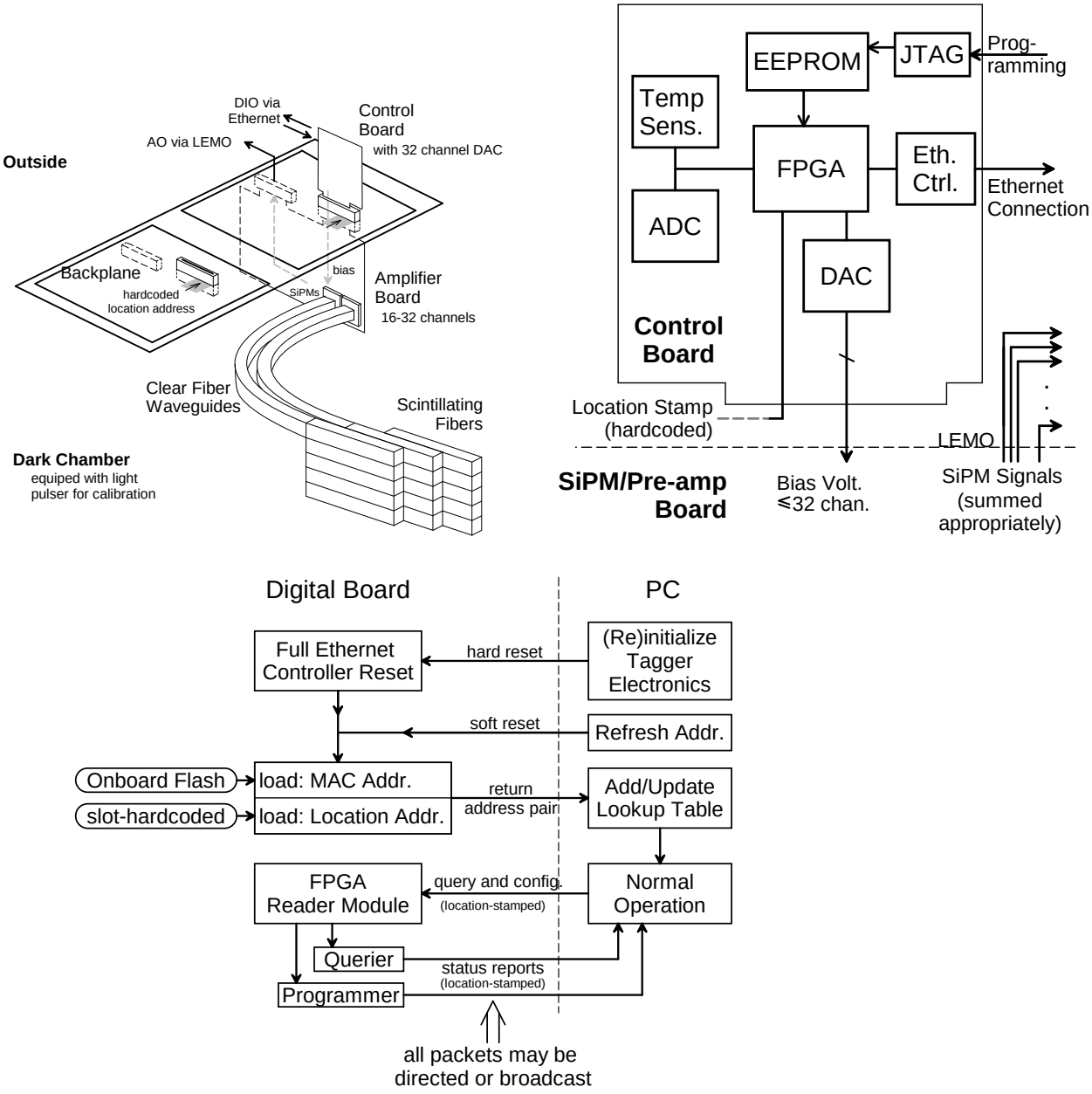

Figure 6: Clockwise from upper left: (1) the analog amplifier and digital control boards are shown schematically along with their input and output sources; (2) a detail of the digital control board design; (3) the tagger control flow along with the startup procedure.

the PCB. In order to avoid long traces carrying fast signals as well as to reduce the manufacturing costs, digital control and analog boards have been made as compact as possible. A three-dimensional rendition of the fully routed digital board is shown in Fig. 7.

The principal challenge in the routing of traces on the digital board has been posed by the densely-packed ball grid array (BGA) of the DAC chip, compounded by strict design rules enforcing large separation of its traces due its capacity to carry voltages up to 200 V. Some connections required shrinking traces to an unusual width of 0.003". In other respects, the board conforms to standard manufacturing schemes. The board has been submitted to a manufacturer to produce a few prototypes for testing. The surface mount components necessary for its population are being procured. The order with Photonique for the SiPMs necessary for the prototype has been placed.

3.3 SiPM Amplifier Board

The layout of the SiPM bias and amplification board is also in its final stages. The board is designed to contain up to 32 SiPM's with individual amplifiers on each, also summed outputs by groups of 5 on the first 30 channels. The plan is to instrument only the first 25 channels on each board with SiPM's for the microscope, and leave the remaining 7 slots for eventual expansion. One reason to do this is that the most expensive component in the system, the DAC chip that provides the individual bias to each SiPM (200 apiece) has 32 outputs, and the extra real estate and components for the additional channels on the amplifier card entail a negligible increment in the electronics cost. An efficient packing design of the 32 SiPM amplifier circuits has been worked out and implemented. Summing circuitry of groups of 5 channels has been designed and laid out [1]. Both the individual amplifier outputs and the summed outputs are available on the output connector of the amplifier board, but only the sum signals and a few of the individual channel output signals are actually routed to LEMO connectors on the interconnect board for delivery to the ADC system. In total, there are 100 sum signals and 20 individual signals for a total of 120 signals from the microscope to be digitized.

The amplifiers are modeled after those provided by Photonique for single photon counting with their SiPMs. The output of the amplifier in response to a single-pixel event is shown by the oscilloscope trace in Fig. 8. The amplifier is designed as a transimpedance device with a nominal gain about 3 $k\Omega$, consisting of two stages: an input amplifier stage based on the BFS 17A transistor and an emitter-follow driver based on the transistor BFT 92. Both of these bipolar transistors are fast devices, with bandwidths of 3 and 5 GHz, respectively. Another second-stage driver circuit is being added to provide a simultaneous independent current source for an open-collector BFS 17A-based summing circuit. This arrangement will allow independent readout of individual channels and their sum.

Work is being conducted on amplifier optimization for the microscope. The goal is to extend the dynamic range to allow running with about 300 photons per pulse without saturation while retaining the ability to increase the gain high enough to resolve individual photon peaks during calibration and setup. The signal decay time introduced by the capacitive coupling of the amplifier to the SiPM is being reduced as far as possible (within the 250 MHz sampling rate of the Flash

[1] Recall that for most energy bins of the tagger microscope, individual vertical channel readout is unnecessary.

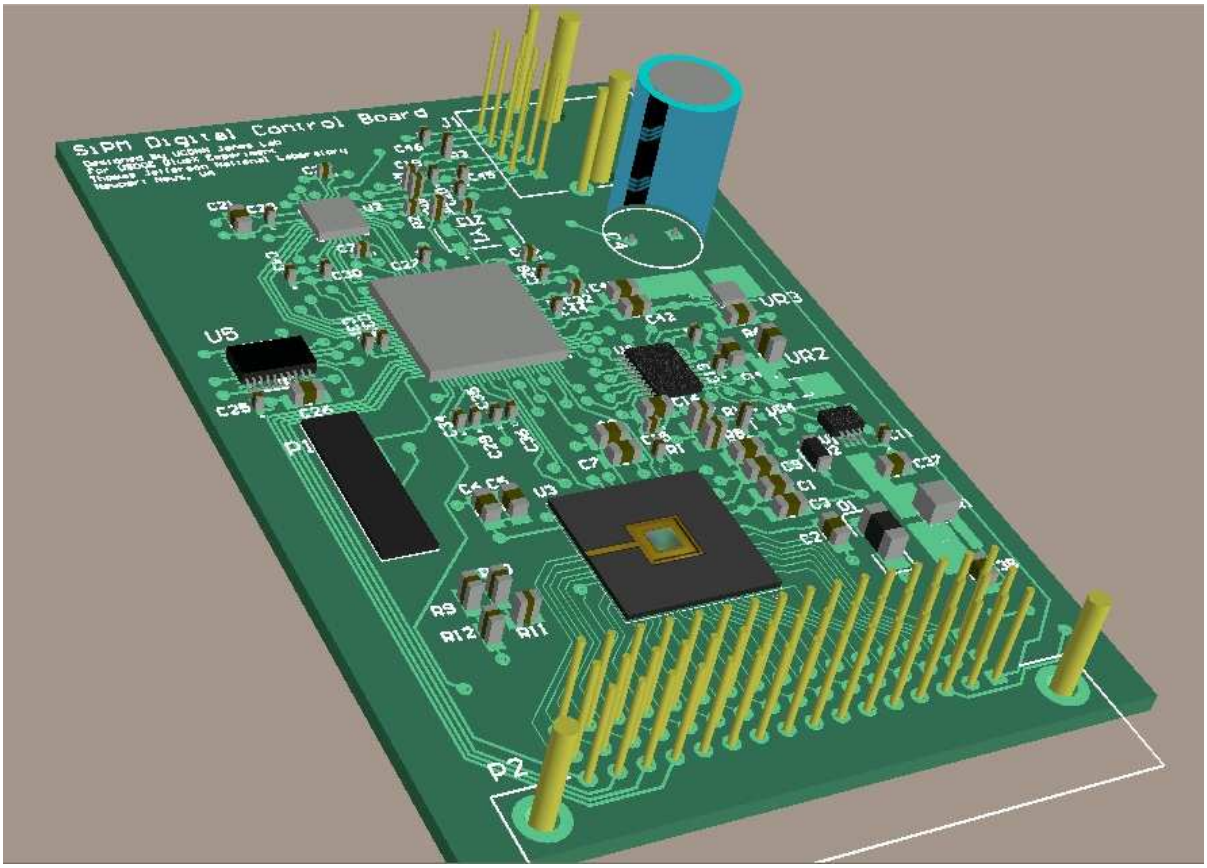

Figure 7: 3D rendering of the digital control electronics board. The pins seen along the lower edge represent the footprint of the elbowed male EuroCard connector. The pins in the upper-right corner are placeholders for the RJ-45 jack to be mounted there. The black pad shown along the left edge is the footprint of the JTAG header. Its placement along this edge gives it easy access from behind the microscope enclosure.

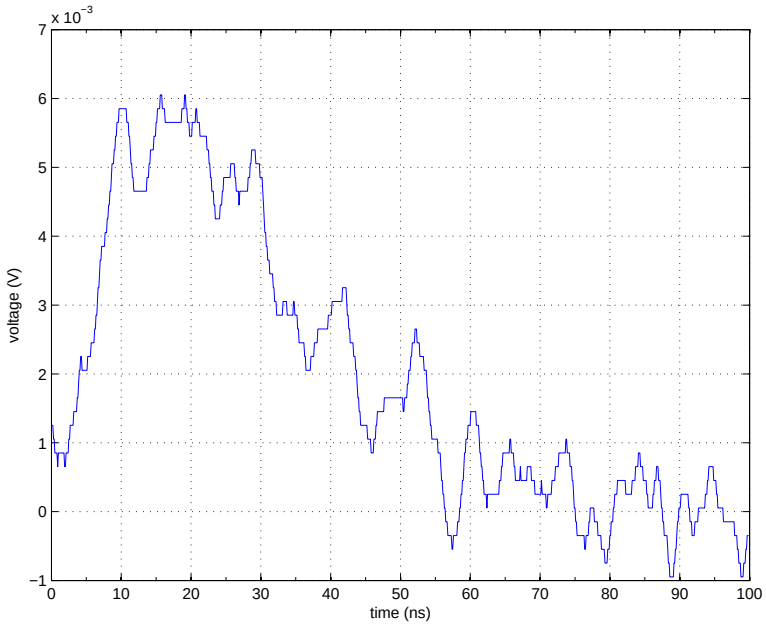

Figure 8: Single-shot output waveform from thermal single-pixel events in the SiPM. This was captured using the amplifier from Photonique configured for single photon counting. Aside from reconfiguring the gain, the long pulse decay time seen in this figure will be decreased substantially in the amplifiers designed for the tagger microscope.

ADC) in order to increase the operating rate per channel. Consistency of amplifier performance from one channel to the next, given the variability of component values is also being investigated.

A few prototypes of each board will be produced and populated for testing and eventual use with the prototype detector, whose construction is proceeding in parallel with the electronics effort.

4 Prototyping the Fiber Hodoscope Fabrication Process

The optics of the tagger microscope consist of a straight segment of scintillating plastic fiber 2 cm long glued to a clear waveguide 50-80 cm in length. The waveguide bends the light out of the plane of the spectrometer, and curves through an arc to direct the light onto the SiPM. There is a small air gap of approximately 1 mm between the end of the waveguide and the active surface of the SiPM. The specified minimum transmission factor for the light within the acceptance of the scintillating fiber reaching the SiPM is 80%. Beside maximizing transmission, optical design must also minimize light leakage between adjacent fibers in order to keep optical cross-talk between channels to a minimum.

The primary source of transmission loss occurs at the joint between the scintillating fibers and the waveguides. Use of optical epoxy is one method to both limit the transmission loss and provide

a stable bond between the scintillating fibers and the waveguides. The optical epoxy 20-3238 from the manufacturer Epoxies Etc., with an index of refraction of 1.54 and a tensile strength of 9,400 psi, has been evaluated for this purpose.

Before the epoxy was applied, the fibers were first carefully cut and the ends polished. To accomplish this task, several successive steps have been developed, each step adding an extra level of refinement to the final result. Fig. 9 shows photographs of a fiber at four major stages in the polishing procedure. Going through all of the steps, from original cleaving of the fiber to the final fine-grit finish takes about two hours of manual labor to complete for a single end of a fiber. Therefore one of the first questions addressed was to see if a rough polish is sufficient to prepare the ends of the fibers to be joined with glue. Several glue joints were made between segments of clear fiber, each made using ends prepared with varying degrees of polish.

Fig. 10 shows two fibers mounted in the alignment jig before gluing (left panel) and after the glue has set (right panel). Transmission testing of each of the glued sample waveguides is being performed to determine if the additional polishing steps are necessary to ensure the required transmission rate.

One of the most time-consuming steps in the preparation for gluing is the cutting of fibers without damage to the surrounding cladding. Attempts at simple and direct cutting of fibers with a scalpel resulted in flayed layers of cladding over a millimeter from the cut. The quality of cut and finish shown in the photographs required the delicate process of removing a ring of cladding layers from the fiber to expose the core before attempting a cut. In a step toward mass-processing of fibers and in a way that protects the cladding, fly-cutting of a bundle of fibers was attempted. Roughly cut segments of fiber were bundled and clamped in a square arrangement with their tips approximately aligned. The bundle was then fixed on the table of a milling machine and the ends cut off smooth using a carbide fly-cutter. The machining parameters of this technique have been perfected, resulting in a quality of cut and polish comparable to several stages of manual work with significantly less labor, as seen in Fig. 11.

One big advantage of bundling is that the cladding of a fiber is held pressed against its neighbor's. Only the outer surfaces of the outer fibers had been visibly peeled away from the core when this technique was used. A permanent set of "sacrificial" fibers can be used in these operations as a protecting layer around the core of the bundle. Only final and quick polishing steps remain after such a bundle is cut with this method. The fly-cutter leaves a fairly smooth, planar surface but visible grains remain as artifacts of the motion of the blade. These are polished off quite easily using traditional methods. The efficiency of this method eliminates the need to rely on the optical epoxy for filling grooves left after a rough polish and provides a consistent and effective method to produce very flat and smooth fiber tips.

Other sources of transmission loss include the attenuation of photons traveling through the waveguide, and reflection at the air gap between the waveguide and the SiPM. These sources produce transmission losses of 8% and 4%, respectively. Quick measurements of glued joints between fibers showed 95±11% transmission. Additional measurements are in progress to ascertain the transmission rate more precisely and to verify its consistency from one joint to the next.

A more significant concern related to the loss of photons along the waveguide is the possibility of their capture in adjacent fiber channels. To prevent this from occurring, the fibers will be coated

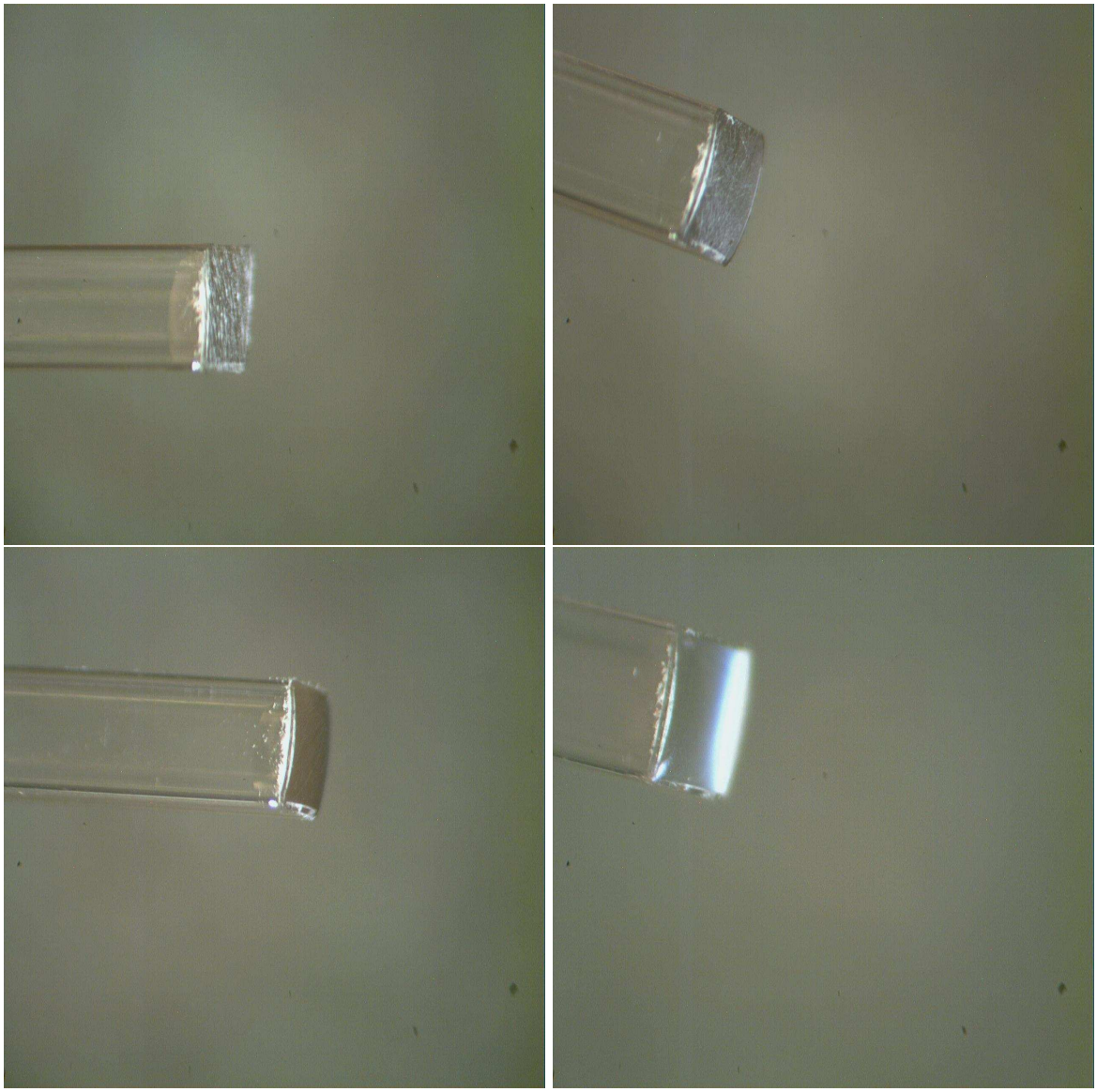

Figure 9: Photographs of the ends of clear plastic fibers of 2×2 mm^2 cross section after cleaving and varying degrees of polish, from rough polish with an emery board (upper left panel), to rough-grit polish (upper right panel), to medium-grit (lower left panel), to fine-grit (lower right panel).

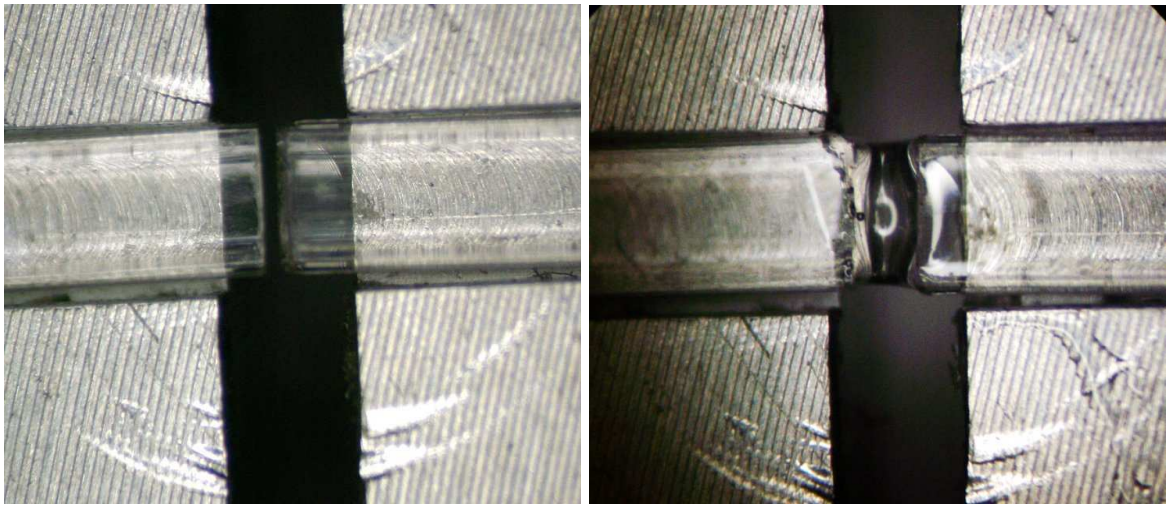

Figure 10: Photographs of an optical fiber joint before (left panel) and after (right panel) the glue has been applied. Note that the volume of glue applied must be carefully controlled to avoid the formation of a bulge at the joint that would interfere with the stacking of the fibers.

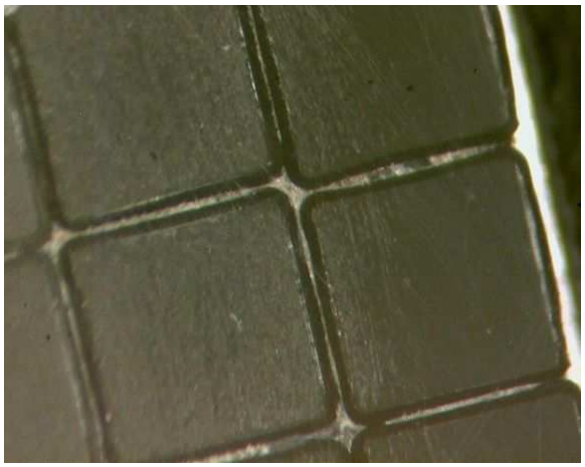

Figure 11: Photographs of some fibers from a bundle after the fly-cutting stage. Note the light vertical scratch marks from the blade.

with a reflective or absorbent material, only a few microns thick. One option is the EMA (extra mural absorber) coating offered by Bicron, the manufacturer of the fibers. Other options include vacuum deposition of opaque coating on the outer cladding of the fibers by a process known as sputtering. Sputtering involves creating a plasma of a specific material then injecting that plasma into a vacuum chamber containing the objects to be coated. The atoms in the cooling plasma then bond to any cool material, forming a thin coating around all exposed surfaces. This technique would permit the choice of a reflective material, which would have the additional feature that it would reflect light from the upstream end of the scintillating fiber. Scintillation photons within the critical angle of the fiber axis but moving away from the waveguide will be reflected back, nearly doubling the photon yield. Additionally, this coating may be less than 1 μm thick, compared to 10-15 μm for the EMA. The sputtering deposition could be performed after the glue junction is made, providing interchannel isolation in that region as well as along the length of the fiber, whereas relying on the manufacturer's EMA coating may result in photons leaking into adjacent channels at the glue joint.

A simpler approach to isolating the fibers is a simple spray-on coating. The advantage of this method is that it costs essentially nothing, since spray paint is a widely available consumer product. An important additional convenience is the ability to apply the coating by the fabrication personnel, avoiding the interruption and delay of submitting the glued fiber pairs to a sputtering facility. The principal concern with this method is the thickness of the deposited layer. However, tests showed that an ostensibly opaque layer was no more than 50 μm thick. While this is quite a bit thicker than the promise of the methods described above, it is not significant on the scale of the fiber thickness and, in the opinion of our research group, well worth the saved expense for the project. This approach requires a separate application of a reflective coating on the tips of the scintillating fibers. Gluing thin pieces of foil with optical epoxy should suffice for this purpose.

The use of any coating changes the optical properties of the waveguide, generally reducing the overall transmission in the fiber channel. For the EMA coating, the manufacturer claims that the effect of the absorbing layer on the outside of the double-clad fibers is to reduce slightly the acceptance of the fiber, without affecting the attenuation length. It would seem that this effect should be the same for either metallic or absorbing coatings.

The 100x5 fiber array will be segmented into into 20 5x5 modules. This segmentation provides the following benefits:

1. easier management of the fiber array during fabrication
2. convenient modularization for maintenance
3. correspondence to segmentation of electronics channels: each SiPM amplifier board contains 25 SiPMs.
4. convenient multiple for even distribution of fibers and uniform placement of un-summed fiber channels.
5. simplified fabrication of each module

The reason for the last item is the following. As the unit of the array modularization, it will be sufficient to stagger the modules to achieve the necessary alignment of the scintillators to the focal plane, , while keeping the ends flush within a 5x5 module. Fiber columns withing the 5x5 module may remain flush with one another with negligible misalignment from the focal plane. Additionally, the reflective coating on the front of the scintillators is very easily applied as a single 5mm x 5mm reflective foil, because the front surface of each module is flat.

The gluing of fibers in the alignment jig shown in Fig. 10 can be done for many fiber pairs simultaneously. A pair of "chimney" blocks that will be used to hold arrays of clear fibers against the SiPM windows in the finished detector can be used during fabrication for precise alignment of scintillating and clear fiber batches and gluing them in sets of 32. The opaque coating will be applied after the individual glue joints have cured. In this way the optical channels are very well isolated. The group is proceeding with the fabrication of a few of these "chimney" blocks in order to test this mass-gluing procedure, and also for the instrumentation of the microscope prototype. Milling the square grooves in plastic materials has already been tested. Automated milling machine instructions are being written for batch machining of the 32 channels per chimney. This procedure will later be applied to the eventual fabrication of 20 such blocks.

5 Mechanical Design

The following general requirements have been set forth for the mechanical design of the tagger microscope.

1. The fibers and SiPMs must be well-sealed from ambient light.
2. Structural elements may not obstruct the electron trajectory to the scintillating fibers. Also, as far as possible, space downstream from the scintillators must be clear.
3. Motorized internal 3-point adjustment of the fiber array plane for remote-controlled alignment with the mid-plane of the electron trajectories.
4. Efficient and decoupled methods for access to electronics and optics must be implemented. At the same time, a simple and effective alignment scheme between these must exist.
5. Sufficient room must be allocated for bending the relatively stiff 2 mm square fiber waveguides.
6. Pulser apparatus for testing the microscope without beam must be designed that brings light flashes of consistent timing and intensity to all fibers.
7. The microscope geometry should allow its relocation within the spectrum of tagged photon energies over as wide a range as possible, at least as high as 10 GeV and as low as 6 GeV.

The scheme for managing the 500 fibers involves segmenting the 100×5 fiber array into 20 modules of 5×5 fibers. Each module is paired with a single amplifier board and a single digital control board. This 5×5 unit also represents a convenient tagger segment for prototyping. The tagger prototype under construction contains one fiber module and one set of electronics boards.

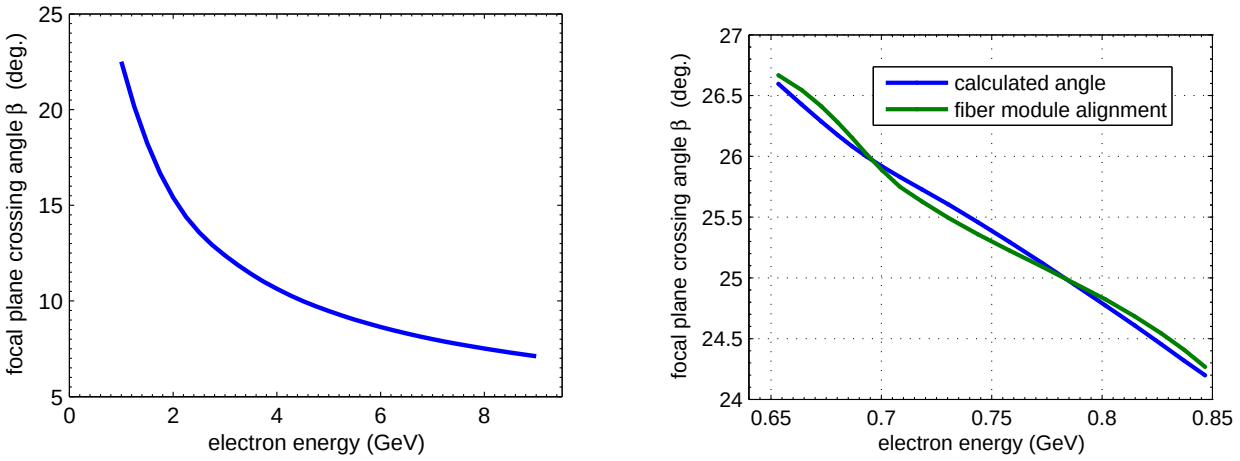

Figure 12: Focal plane crossing angle of the electrons. The closest alignment of fiber-modules (tested with CAD) is shown for comparison. The standard deviation between these is 0.02°, compared with the angular acceptance of a fiber for off-axial tracks of ±1°.

Fig. 13 shows a cut-away view of the tagger microscope enclosure, showing all of the fiber modules but only a single clear fiber in place, for purposes of illustration. The alignment of the axis of the fibers with the incident electron trajectories is made possible by individually fixing them to a pair of rails. Each module is mounted on a fixture with sliding attachments to the two rails so that the incidence angle can be individually adjusted. As shown in Fig. 12, the angle β at which electron trajectories cross the focal plane in the range of useful photon energies 3-12 GeV spans from 8 to about 60 degrees. The rails can rotate with respect to one another, deviating from this parallel arrangement. It can be shown that the alignment of the fiber modules along the rails in this configuration allows a small angular shift from one fiber module to the next, satisfying to the necessary extent the alignment with the electron trajectories. This is important at the high-energy end of the tagged photon spectrum, where the crossing angles of the electron trajectories vary rapidly with energy. The right panel in Fig. 12 shows the alignment capability of the microscope design as tested with a CAD program. There is a negligible standard deviation of 0.02° between the nominal crossing angle and that allowed by the railing geometry.

The simplest design for a 3-point adjustable plane on which the fiber modules would be mounted is to have it rest directly on motor shafts positioned vertically. The threaded shafts can lift and lower their respective points by passing through threaded holes in the elbow assembly that keeps that point fixed but able to rotate in order to accommodate changes in elevation at the other two support points.

The 83 oz·in Lin Engineering 4118L-01 (1.9") Step Motor has been chosen for this design. The unit and its driver are inexpensive, yet its torque is more than sufficient for the friction and load of the railing system. This motor has been tested with its driver on the bench. It is very simple to control and provides a small step size of 1.87° with a very high torque hold in any position as

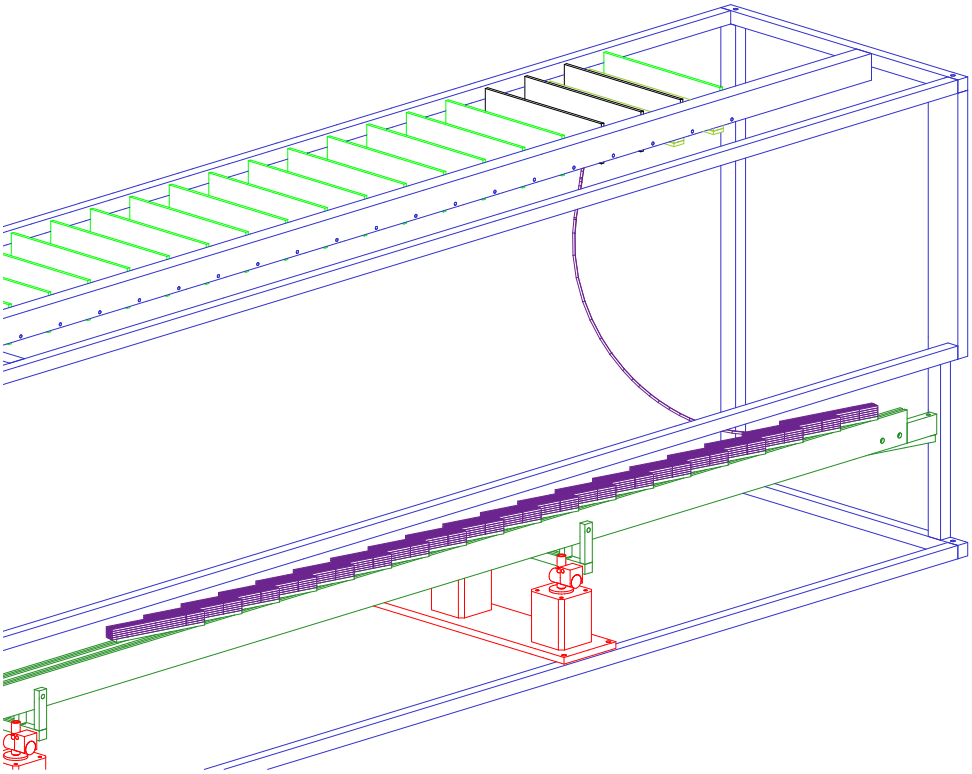

Figure 13: A three-dimensional view of the microscope with the side panels and control boards removed. A single waveguide fiber is shown.

long as the power supplies are on. This will guarantee that the fiber array orientation is fixed once proper alignment to the focal plane has been found. Using a common screw pitch of 20 threads/in gives an elevation change of only 10 μm/step. The maximum speed of the motor is 1500 steps/min. Staff in the University of Connecticut Physics machine shop have confirmed that the shaft of these motors can be threaded to meet the requirements of the microscope design.

The scheme of modules and railing described above will be prototyped prior to beginning full-scale construction. The microscope prototype will simply be a single fiber module set up on a reduced-length railing system in a smaller enclosure with room for one set of electronics boards. This is one complete replica of the 20 segments, 5% of the full microscope. This approach allows full testing of all mechanical and electronics ideas in the prototype detector. The mechanical design shown here is currently being rescaled for the prototype construction. As mentioned above, some machining tests have been carried out and fiber array fabrication techniques are now relatively mature.

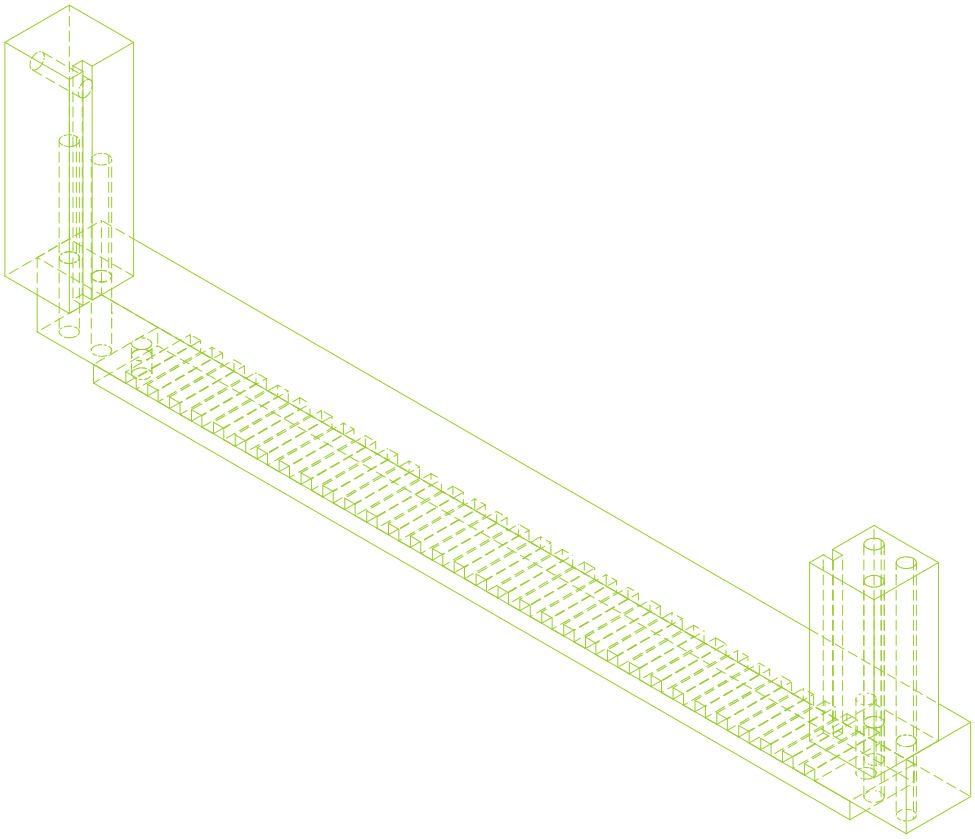

Figure 14: A "chimney" assembly, so called for its array of chimney-like channels through which square fibers descend to the SiPM. Card guides are provided for the insertion of the SiPM/amplifier boards, creating a two-dimensional reference. Alignment of SiPMs to fibers in the remaining vertical direction is guaranteed by the PCB layout: on-board holes for backplane connector attachment and vias for SiPM insertion are set to within 0.001" tolerance. The SiPM manufacturer guarantees active windows placement to comparable precision.

6 Recommendations

The following recommendations are offered as a result of these studies.

1. Test the prototype electronics boards, and choose one of each for mounting in the prototype detector.
2. Assemble and test the assembled prototype detector with a built-in prototype pulser.
3. Take the prototype microscope to a test beam facility and test it with real electrons.

References

[1] I. Senderovich, C.R. Nettleton and R.T. Jones, ‘ ‘Prototype Scintillating Fiber Tagger Microscope Design and Construction” GlueX-doc-1074 (2008).

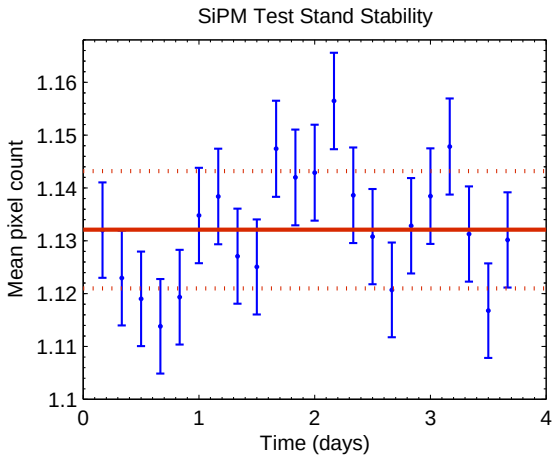

Figure A.1: Average number of photons detected per pulse during a continuous 4-day run with the test stand. The mean detected counts are averaged over 4-hour periods for each data point. Error bars are statistical only. The solid curve shows the 4-day average, while the dashed curves show an upper limit on the systematic deviation throughout the run at 90% confidence level.

Appendix

A Test Stand Stability

The reliability of the fiber-optics test stand required verification. Temperature and voltage drifts affecting the LED light output, as well as possible variation in ambient light, were the principal concerns. Thus a simple stability test was performed. The stand was set up to acquire data continuously over the course of several days. The data were then examined in 4-hour slices, searching for drifts in the mean photoelectron count. Indeed, no statistically significant drifts in pulser performance were detected, as can be seen in Fig. A.1.

B Search for Light Source for Tagger Test Pulser

A search for a fast light source was conducted in order to find the best unit for the test pulser inside the microscope. Being built for timing tests, that pulser system requires the fastest possible source, regardless of wavelength. To that end, a blue Panasonic Semiconductor LNG992CFBW and two laser diodes were acquired: ADL-63054TL and ADL-65055TL of wavelengths 635 nm and 655 nm respectively. Several stock LEDs were also tested and compared with these new units. These included the blue-green Agilent (Avago Technologies) HLMP-CE30-QTC00, yellow Fairchild MV8304 and red (Fairchild MV8104).
A direct pulse shape measurement was made in the following way. A Hamamatsu SiPM (described above) was mounted in the test box, and read out without amplification. This was

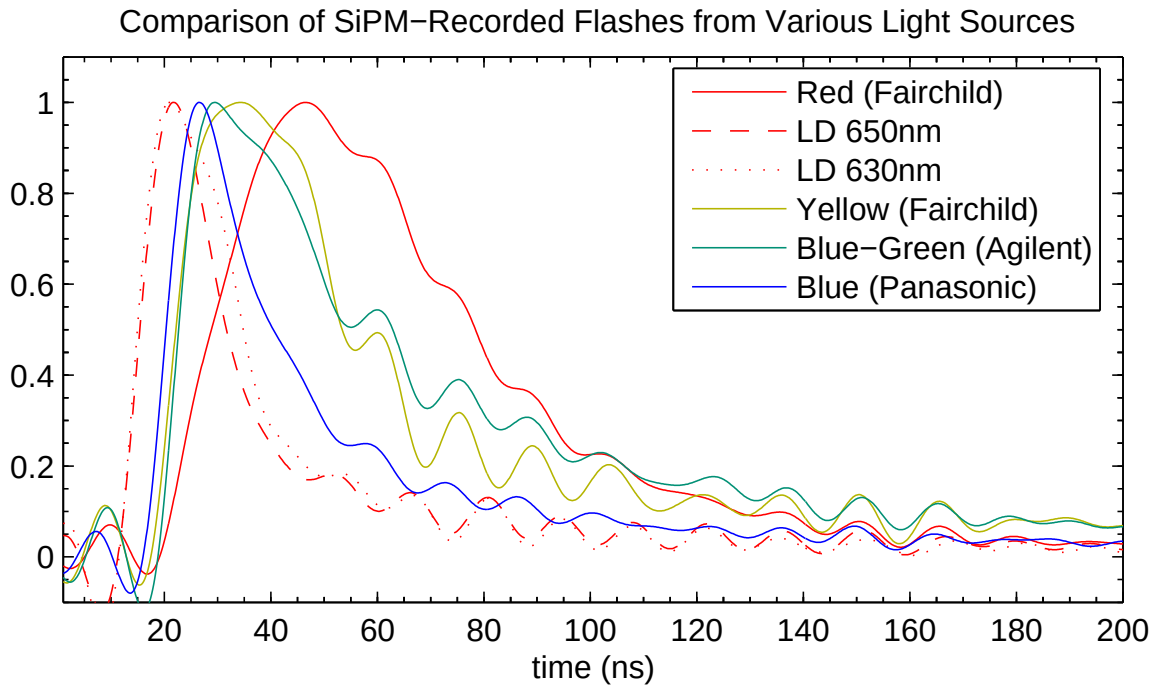

Figure B.1: A comparison of the light sources in terms of their speed (note the normalization of their intensities.) These measurements were made by reading the signal directly from the Hamamatsu SiPM to avoid the shape distortion of the amplifier. Shaping due to the input pulse from the pulser has been taken out. It is thought that the remaining width among the faster sources like the laser diodes are due to the response function of the SiPM.

possible due to the high gain of this sensor. Fig. B.1 provides the results of these measurements. The shape of the input voltage function from the pulser electronics has been taken out of these measurements by deconvolution. The width of the functions from the faster sources, the Panasonic LED and the two laser diodes is similar. It is thought to be entirely from the characteristic response function of the SiPM.